Materials International
Open-Access Journal (ISSN: 2668-5728)

Article
Volume 8, Issue 1, 2026, 4
https://doi.org/10.33263/Materials81.004

Metal-Doped BN Nanocages as Smart Sensors for NO Adsorption: A DFT Study

Fatemeh Mollaamin [1,*]

[1] Department of Biomedical Engineering, Faculty of Engineering and Architecture, Kastamonu University, Kastamonu, Turkey
* Correspondence: fmollaamin@kastamonu.edu.tr;

Received: 1.09.2025; Accepted: 20.11.2025; Published: 10.03.2026

Abstract: The partial density of states (PDOS) can evaluate a determined charge assembly between gas molecules and $B_4(X)N_{10}$, which indicates the competition among dominant complexes of Sc, V, and Cr. Based on NQR analysis, X-doped on B_5N_{10} has shown the lowest fluctuation in electric potential and the highest negative atomic charge, including 0.5970 coulomb (chromium), 0.7392 coulomb (vanadium), and 0.8259 coulomb (scandium), respectively, which have presented the highest and the lowest tendency for being the electron acceptors. Furthermore, the reported results of NMR spectroscopy have exhibited that the yield of electron accepting for doping atoms on the $B_4(X)N_{10}$ through gas molecules adsorption can be ordered as: Cr >V≈SC. Regarding IR spectroscopy, doped nanocages of B_4**(**Sc**)**N_{10}, $B_4(V)N_{10}$, and B_4**(**Cr**)**N_{10}, respectively, have the most fluctuations and the highest adsorption tendency for gas molecules, which can address specific questions on the individual effect of charge carriers (gas molecule-nanocage), as well as doping atoms on the overall structure. Based on the results of ΔG_R^o amounts in this research, the maximum efficiency of Sc, V, Cr atoms doping of B_5N_{10} for gas molecules adsorption depends on the covalent bond between NO molecules and B_4**(**X**)**N_{10} as a potent sensor for air pollution removal.

Keywords: air pollution; smart materials; gas sensor; transition metals; quantum computation.

1. Introduction

BN-nanomaterials have been used owing to their unparalleled specifications of eco-friendly attributes for pollutant adsorption and semiconducting properties [1,2]. Boron nitride nanomaterials usually exhibit semi-leading behavior, which is considered a proper alternative to carbon nanotubes. The properties of boron and nitrogen atoms, which are the first neighbors of carbon in the periodic table, make boron nitride an interesting subject of numerous studies [3].

Various physical shapes of boron nitride (BN)-based nano adsorbents such as nanoparticles, fullerenes, nanotubes, nanofibers, nanoribbons, nanosheets, nanomeshes, nanoflowers, and hollow spheres have been broadly considered possible adsorbents owing to their exceptional characteristics such as large surface area, structural variability, great

chemical/mechanical strength, abundant structural defects, high reactive sites, and functional groups [4,5].

Adsorption of charged adsorbates alters the double layer and the potential at the outer Helmholtz plane, thereby influencing the adsorption rates of both anodic and cathodic reactions. The first three modes are intimately related to adsorption, and the double layer involves interaction of the adsorbates and the intermediate products. These compounds have been formed during partial electrochemical reactions and during the interaction of adsorbed intermediates with organic molecules, which can either inhibit or enhance the electrode reaction rate [6,7].

The progress of highly selective and sensitive gas sensors is crucial for sensing toxic pollutants, such as carbon monoxide. Recently, the scientists investigated the adsorption of CO molecules on Ni_6−xCux (x = 0–6) clusters supported on hexagonal boron nitride quantum dots with nitrogen vacancies through density functional theory (DFT) computations. The adsorption energy and charge transfer calculations indicated that the Ni_6 and N_{i6}−xCux (x = 2 and 3) complexes show the strongest CO binding and highest charge transfer, suggesting them as appropriate materials for CO gas detection [8].

Furthermore, the adsorption behavior of a NO molecule on a defective h-BN monolayer is studied using density functional theory. The results indicated that the initial configuration of N and O atoms over vacancy defects plays a key role in determining whether the NO molecule is adsorbed on the h-BN monolayer via covalent or ionic bonding. In the case of mono-vacancy, the O–N configuration of the NO gas resulted in lower total energy (Etotal) compared with the N–O configuration [9].

Particularly, this research work aims to assess the influences of doping atoms of Sc, V, and Cr on the B_5N_{10} for increasing gas detection through measurement of some parameters containing charge transfer, electric potential, electromagnetic and thermodynamic properties, surface area, functional group, and to examine the removal of selected toxic gas molecules, including nitrogen monoxide, during the adsorption process. The aim of this research article is a comparative DFT assessment of dopant effects on NO adsorption.

2. Materials and Methods

2.1. Adsorption of NO on $B_4(X)N_{10}$.

The goal of this study is to remove toxic gas molecules, including NO, from air through an eco-friendly approach by using (Sc, V, Cr)-doped B_5N_{10} (Figure 1).

Boron nitride nanocage was modeled in the presence of doping atoms of scandium, vanadium, and chromium, which can increase the gas sensing potential of BN-nanocage. In our research, sample characterization was performed by CAM–B3LYP–D3 /EPR–3, LANL2DZ level of theory.

Figure 1 shows the process of NO adsorption on the $B_4(X)N_{10}$ surface, which leads to the formation of complexes containing NO@ $B_4(Sc)N_{10}$, NO@ $B_4(V)N_{10}$, and NO@ $B_4(Cr)N_{10}$ by molecular modeling computations.

The charge distribution of the mentioned complexes is calculated due to the Bader charge analysis [10]. The trapping of NO molecules by $B_4(X)N_{10}$ (X= Sc, V, Cr) was successfully incorporated due to binding formation consisting of N→ Sc, N→ V, N→ Cr (Figure 1).

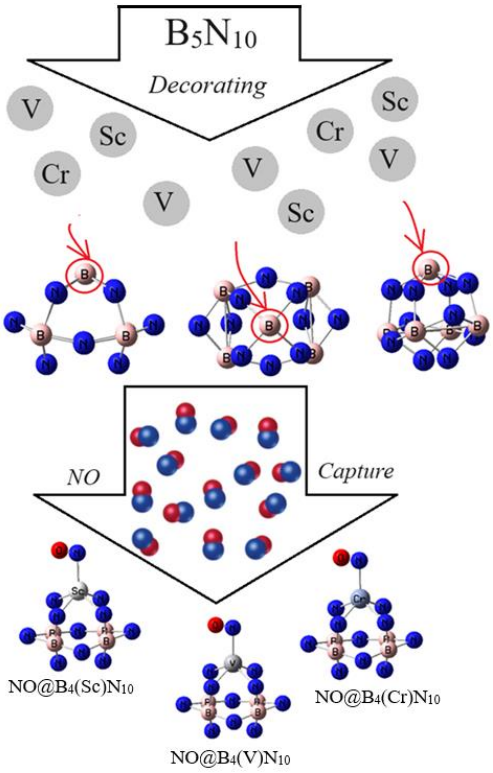

Figure 1. Application of B_4**(**X**)**N_{10} towards adsorption of gas molecules of NO and formation of complexes: NO@B_4**(**Sc**)**N_{10}, NO@B_4(V)N_{10}, NO@B_4**(**Cr**)**N_{10} using CAM–B3LYP–D3/6–311+G (d,p), LANL2DZ calculation. (Note: the sign of adsorption is shown with @).

2.2. Application of the density functional theory approach.

All calculations in this paper were performed with the first-principles method based on the density functional theory (DFT) method. The geometries optimization and vibrational frequencies analysis of the models were calculated using DFT with the hybrid exchange-correlation functional B3LYP and 6-311+G(d,p) basis sets [11] due to Gaussian 16 revision C.01 computational software [12] and GaussView 6.1 graphical program [13].

In this investigation, the computations have been launched by the Coulomb-attenuating method–(Becke, 3-parameter, Lee-Yang-Parr) [CAM–B3LYP–D3] level of theory. This highlights the importance of considering the electronic correlation and dispersion effects in accurately predicting polarizabilities [14]. Dispersion forces were considered under the "DFT-D3" method of Grimme with Becke–Johnson damping with multiplicity of +1 and convergence on RMS density matrix=1.00D-08 and convergence on MAX density matrix=1.00D-06 [15].

In this investigation, the Onsager model, which was developed by Frisch, Wong, and Wiberg, utilizes spherical cavities. Even though this implies a less accurate description of the solute-solvent interface, this approximation simplifies the evaluation of energy changes during geometry optimizations and frequency analyses. In fact, a cavity must have a physical sense, as in the Onsager model, and a mathematical ability, as is often the case in other descriptions of solvent effects [16]. On the other hand, the cavity must exclude the solvent and define its boundaries as the most probable region of the solute charge distribution [17].

As revealed by DFT-based analysis, the potency of B4(X)N10 for grabbing NO molecules was determined mainly by the electronegativity of the functional groups, as well as the interaction between the B_4(X)N_{10} and the NO molecules.

3. Results and Discussion

One of the most dominant gas pollutants in the air is nitrogen monoxide. The data has evaluated the efficiency of boron nitride nanocage doped with Sc, V, and Cr for gas detection. In fact, it can be remarked that the chemisorptive nature of the bond among the gas molecules with boron and nitrogen elements through the equilibrium distribution of doping atoms, B_5N_{10}, and a monolayer attribute.

3.1. PDOS & electronic evaluation.

The electronic structures of NO adsorption using X (X= Sc, V, Cr)-doped B_5N_{10} as the selective sensor for detecting and grabbing gas molecules in the air have been illustrated using CAM–B3LYP–D3/6–311+G (d,p), LANL2DZ level of theory.

Figure 2 (a,b,c) shows the projected density of state (PDOS) of NO@B_4**(**X**)**N_{10} through gas molecule adsorption. The appearance of the energy states (*p*-orbital) of N, O, and (*d*-orbital) of Sc, V, Cr within the gap of B_4**(**X**)**N_{10} induces the reactivity of the system. It is clear from the figure that after trapping with gas molecules, there is a significant contribution of *d*-orbital in the unoccupied level. Therefore, the curve of partial PDOS describes that the *p* states of N atoms in gas molecules and *d*-orbital in Sc, V, Cr transition metals in B_4**(**X**)**N_{10} are overcome due to the conduction band (Figure 2a–c). A distinguished adsorption trait might be seen in NO@ B_4**(**X**)**N_{10} because of the potent interaction between the *p* states of the nitrogen atom in gas molecules with *d* states of Sc, V, and Cr in B_4**(**X**)**N_{10} complexes.

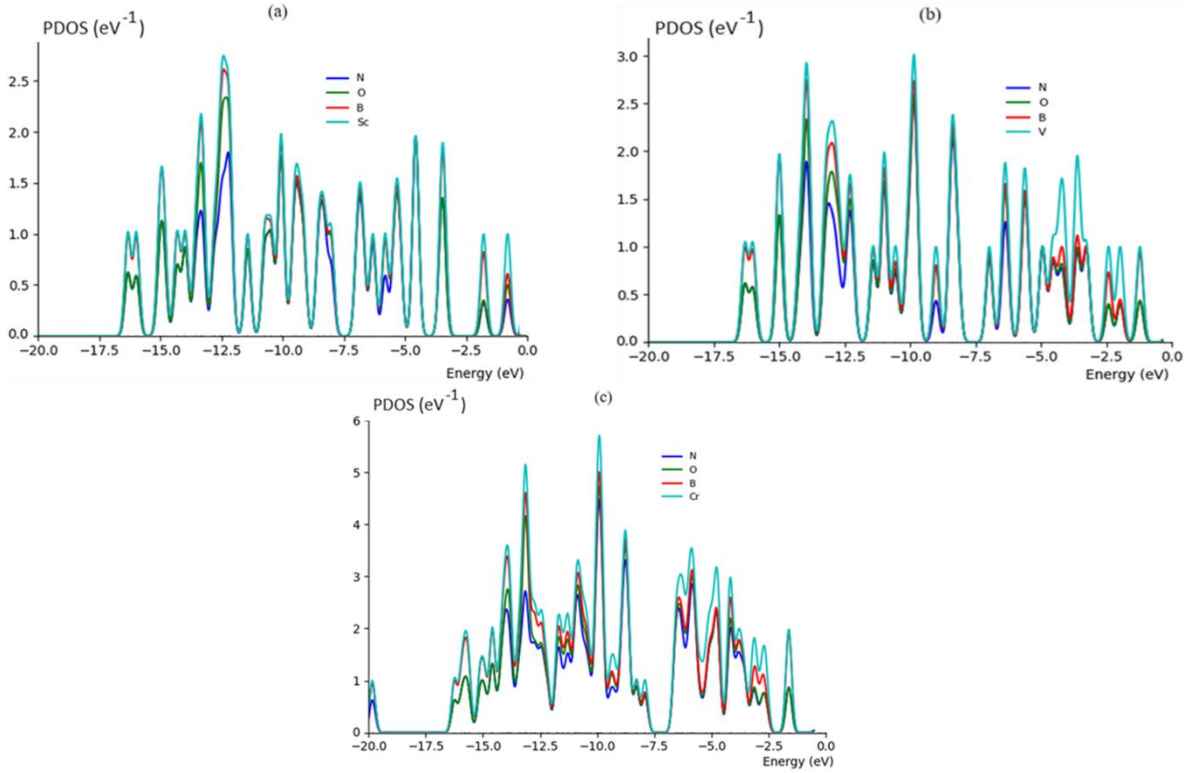

Figure 2. PDOS of gas molecules of NO adsorbed on B_4**(**X**)**N_{10} including **(a)** NO@ B_4**(**Sc**)**N_{10}; **(b)** NO@B_4**(**V**)**N_{10}; **(c)** NO@ B_4**(**Cr**)**N_{10} complexes by CAM–B3LYP–D3/6–311+G **(d,p)**, LANL2DZ. (Note: the sign of adsorption is shown with @).

Figure 2(a,b,c) shows that NO@B_4**(**Sc**)**N_{10}, NO@B_4**(**V**)**N_{10}, and NO@B_4**(**Cr**)**N_{10} complexes through gas molecules adsorption, respectively, have the most contribution at the middle of the conduction band between –5 to –15 eV, while contribution of boron and nitrogen

states are enlarged and similar together, and adsorbing of NO depicts interfacial electronic of the B_4N_{10} for selection of this gas. NO@B_4**(**Sc**)**N_{10} has indicated one sharp peak around –12.5 eV for Sc in Figure 2 (a), while NO@B_4**(**V**)**N_{10} (Figure 2b) and NO@B_4**(**Cr**)**N_{10} complexes (Figure 2c) have exhibited two sharp peaks around –10 and –14.5 eV for V and Cr atoms, respectively. Therefore, the order potency of gas adsorption by doping atoms of Sc, V, and Cr on B_4**(**X**)**N_{10}, based on the PDOS, might be shifted as: B_4**(**Cr**)**N_{10}> B_4**(**V**)**N_{10}> B_4**(**Sc**)**N_{10}.

3.2. Insight into nuclear quadrupole resonance.

As the electric field gradient (EFG) at the citation of the nucleus in NO is allocated by the valence electrons twisted in the attachment with close nuclei of B_4**(**X**)**N_{10} through trapping of gas molecules, the nuclear quadrupole resonance (NQR) [18] frequency at which transitions occur is particular for NO@B_4**(**X**)**N_{10} complexes (Table 1).

In this research work, the electric potential as the quantity of work energy through carrying over the electric charge from one position to another position in the essence of the electric field has been evaluated for NO@ B_4**(**Sc**)**N_{10}, NO@B_4**(**V**)**N_{10}, NO@ B_4**(**Cr**)**N_{10} complexes (Table 1).

Table 1. The electric potential (a.u.) and Bader charge (e) through NQR calculation for NO@ B_4**(**Sc**)**N_{10}, NO@ B_4**(**V**)**N_{10}, and NO@B_4**(**Cr**)**N_{10} complexes using CAM–B3LYP–D3/EPR–3, LANL2DZ calculation.

NO@ B_4(Sc)N_{10}			**NO@ B_4(V)N_{10}**			**NO@ B_4(Cr)N_{10}**		
Atom	**Q**	**E_p**	**Atom**	**Q**	**E_p**	**Atom**	**Q**	**E_p**
N1	–0.062	–18.243	N1	–0.036	–18.209	N1	–0.100	–18.243
O2	–0.117	–22.197	O2	–0.116	–22.195	O2	–0.095	–22.210
B3	0.099	–11.266	B3	0.139	–11.268	B3	0.115	–11.274
N4	0.005	–18.260	N4	–0.046	–18.277	N4	–0.032	–18.274
N5	–0.053	–18.247	N5	–0.074	–18.265	N5	–0.082	–18.275
B6	0.158	–11.271	B6	0.156	–11.269	B6	0.111	–11.274
B7	0.100	–11.269	B7	0.132	–11.266	B7	0.120	–11.275
B8	0.143	–11.272	B8	0.155	–11.269	B8	0.116	–11.276
N9	–0.044	–18.256	N9	–0.048	–18.258	N9	–0.032	–18.266
N10	–0.047	–18.247	N10	–0.073	–18.264	N10	–0.099	–18.282
N11	–0.232	–18.275	N11	–0.201	–18.267	N11	–0.140	–18.264
N12	–0.269	–18.297	N12	–0.218	–18.268	N12	–0.140	–18.262
N13	–0.205	–18.283	N13	–0.189	–18.265	N13	–0.134	–18.261
N14	–0.269	–18.297	N14	–0.220	–18.267	N14	–0.144	–18.264
Sc15	0.826	–9.380	V15	0.739	–12.498	Cr15	0.597	–14.393
N16	–0.026	–18.248	N16	–0.055	–18.261	N16	–0.029	–18.263
N17	–0.005	–18.264	N17	–0.043	–18.274	N17	–0.026	–18.268

In Table 1, the Bader charge and electronic potential properties of Sc, V, Cr, and B, N in B_4**(**X**)**N_{10} and N, O of NO molecules trapped on doped-boron nitride nanocages have been investigated. The amounts indicate that as the negative charge of different atoms increases, the electric potential resulting from NQR calculations increases. Moreover, the doping atoms of Sc (15), V(15), and Cr(15) on the B_5N_{10} have shown the most potential for accepting the electron from the electron donor of N(1) and O (2) in NO adsorbed on the B_4**(**X**)**N_{10} (Table 1).

Furthermore, in Figure 3 (a–f), it has been sketched the electric potential of nuclear quadrupole resonance for some atoms of Sc, V, Cr / B, N in B_4**(**X**)**N_{10} and N, O of gas molecules trapped on doped-boron nitride nanocages which has been calculated by CAM–B3LYP–D3/EPR–3, LANL2DZ.

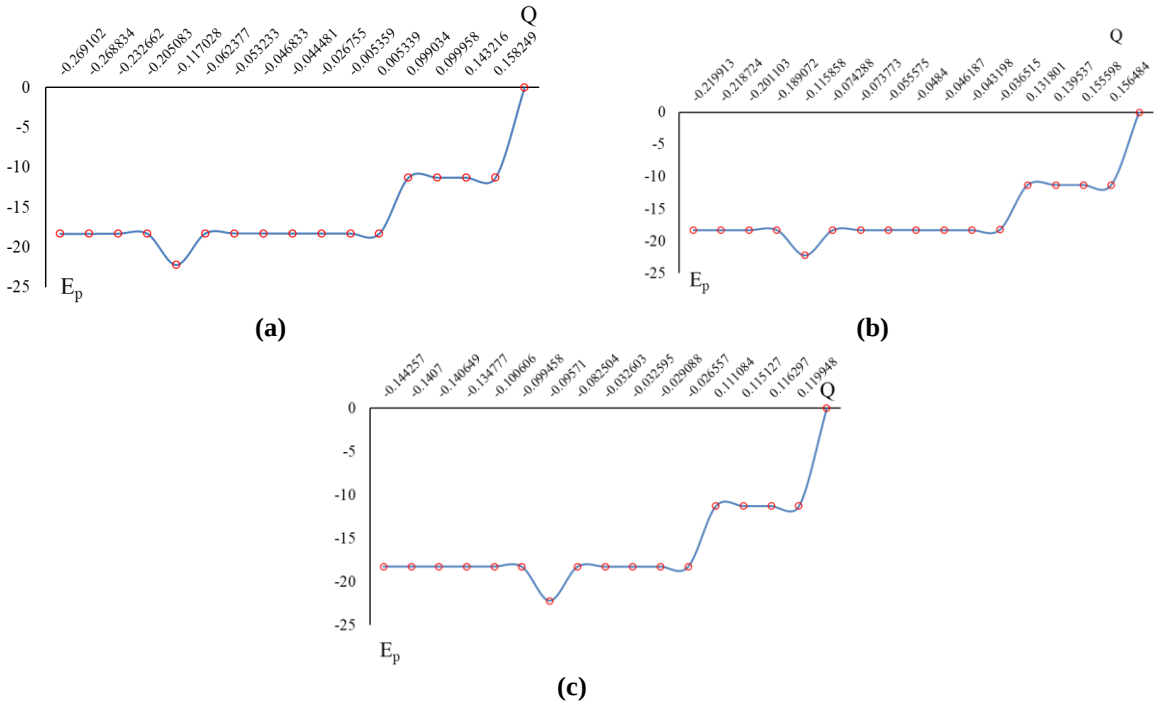

Figure 3. Electric potential (a.u.) versus Bader charge (coulomb) through NQR calculation for **(a)** NO@ B_4**(**Sc**)**N_{10}; **(b)** NO@ B_4**(**V**)**N_{10}; **(c)** NO@B_4**(**Cr**)**N_{10} complexes by CAM–B3LYP–D3/EPR–3, LANL2DZ. (Note: the sign of adsorption is shown with @).

In Figures 3 (a) and (b), the behavior of NO adsorption on the B_4**(**Sc**)**N_{10} and NO@B_4**(**V**)**N_{10}, respectively, is characterized by the analogous high sensitivity based on the relation coefficient of R^2 = 0.9314 and R^2 = 0.9591. Adsorption of NO on the B_4**(**Cr**)**N_{10} in Figure 3 (c) has illustrated the highest sensing with R^2 = 0.9332.

It's vivid that the curve of B_4**(**X**)**N_{10} is waved by NO molecules. The fluctuated peaks for electric potential have been shown around NO trapping on the B_4**(**X**)**N_{10}, which demonstrate the electron accepting specifications of nitrogen and oxygen versus the scandium, vanadium, and chromium doped on the B_4N_{10} (Figure 3a,b,c). Besides, it can be considered that transition metals, such as ferromagnetic semiconductors in the functionalized B_4N_{10}, might have more impressive sensitivity for accepting the electrons from NO by Sc, V, and Cr in the process of the adsorption mechanism.

Table 1 shows that scandium-doped B_5N_{10} has the lowest fluctuation between Bader charge versus electric potential extracted from NQR parameters in NO@ B_4**(**Sc**)**N_{10}, which can be an appropriate option with the highest tendency for electron accepting in the adsorption current (Table 1). In addition, chromium with 0.5970 coulomb and vanadium with 0.7392 coulomb, respectively, have presented the highest and the lowest tendency for being the electron acceptors. In fact, the uptake of gas molecules has been known to be associated with B_4**(**X**)**N_{10}, indicating that the adsorbed NO molecules in the X-doped nanocage can be internalized through a different pathway from the pristine nanocage.

3.3. Analysis of nuclear magnetic resonance spectra.

Based on the resulting amounts, nuclear magnetic resonance (NMR) spectra of B_4**(**X**)**N_{10} (X= Sc, V, Cr) as the potent sensor for adsorbing toxic gas molecules of NO can unravel the efficiency of B_4**(**X**)**N_{10} for detecting and removing these hazardous gases in air as an eco-friendly approach.

From the DFT calculations, the chemical shielding (CS) tensors in the principal axes system have been obtained to estimate the isotropic chemical shielding (CSI) and anisotropic chemical shielding (CSA) [19,20]:

$$\sigma_{iso} = (\sigma_{11} + \sigma_{22} + \sigma_{33})/3 \quad (1)$$

$$\sigma_{aniso} = \sigma_{33} - (\sigma_{22} + \sigma_{11})/2 \quad (2)$$

The NMR data of isotropic (σ_{iso}) and anisotropic shielding tensors (σ_{aniso}) of gas molecules trapped in the B_4**(**X**)**N_{10} towards formation of NO@B_4**(**Sc**)**N_{10}, NO@ B_4**(**V**)**N_{10}, and NO@ B_4**(**Cr**)**N_{10} complexes have been computed by the Gaussian 16 revision C.01 program package and are shown in Table 2.

Table 2. Data of NMR shielding tensors for selected atoms of NO@ B_4**(**Sc**)**N_{10}, NO@B_4**(**V**)**N_{10}, and NO@B_4**(**Cr**)**N_{10} complexes using CAM–B3LYP–D3/6–311+G (d,p), LANL2DZ calculation.

NO@B_4(Sc)N_{10}			**NO@B_4(V)N_{10}**			**NO@B_4(Cr)N_{10}**		
Atom	**σ_{iso}**	**σ_{aniso}**	**Atom**	**σ_{iso}**	**σ_{aniso}**	**Atom**	**σ_{iso}**	**σ_{aniso}**
N1	3288.96	12004.50	N1	8364.44	27502.90	N1	657.46	449.15
O2	3784.83	14745.07	O2	18183.11	59763.77	O2	638.05	829.81
B3	45.32	102.76	B3	117.84	562.2156	B3	73.15	59.20
N4	718.03	9476.56	N4	4204.74	19733.21	N4	864.67	935.73
N5	2082.33	7477.11	N5	6249.23	18732.22	N5	663.8211	1162.01
B6	78.50	120.66	B6	178.28	349.74	B6	73.63	64.90
B7	71.78	105.56	B7	160.30	571.58	B7	70.66	58.23
B8	87.30	63.44	B8	139.22	323.74	B8	67.77	55.83
N9	247.05	1130.01	N9	4148.15	10938.01	N9	194.59	867.75
N10	777.90	7170.48	N10	3592.00	14968.85	N10	637.10	1350.34
N11	1036.46	2615.44	N11	5847.52	9357.01	N11	739.01	891.46
N12	722.49	2826.85	N12	1166.50	8750.80	N12	648.83	703.63
N13	1101.54	1740.61	N13	4231.35	9407.75	N13	686.99	715.76
N14	645.32	2891.22	N14	263.18	9470.19	N14	708.80	622.45
Sc15	603.72	722.60	V15	6179.22	3771.37	Cr15	7806.68	2373.72
N16	645.24	4055.32	N16	1944.78	10094.87	N16	309.99	704.31
N17	207.26	6677.00	N17	10575.45	13849.00	N17	1013.79	1526.37

In Table 2, NMR data have reported the notable amounts for NO, which were adsorbed on the B_4**(**X**)**N_{10} as the selective sensor for detecting gas molecules in air. The observed increase in the chemical shift anisotropies spans for N(1) and O(2) atoms of NO adsorption on the B_4**(**X**)**N_{10}. The observed weak signal intensity near the parallel edge of the nanocage pattern may be due to boron binding-induced non-spherical distribution of these complexes.

It is remarkable that doping of Sc, V, and Cr on B_4N_{10} might promote the stability of the nanocage that results in enhanced magnetic alignment of complexes. Interestingly, the reported results show that Sc, V, and Cr elements can be optimized to achieve optimal alignment of the nanocage in the presence of an applied magnetic field.

In fact, the adsorption of NO can introduce spin polarization on the B_4**(**X**)**N_{10}, which indicates that these surfaces might be applied as a magnetic scavenging surface as a gas detector. Isotropic and anisotropic shielding fluctuate with the occupancy in the electron-accepting gas molecules trapped on the atom-doped boron nitride nanocage.

Figure 4 (a,b,c) exhibited the same tendency of shielding for boron and nitrogen; however, a considerable deviation exists from doping atoms of Sc (15), V (15), Cr (15), Co

(15), Cu (15), Zn(15) through interaction with N (1) and O (2) of NO during adsorbing on the B_5N_{10}.

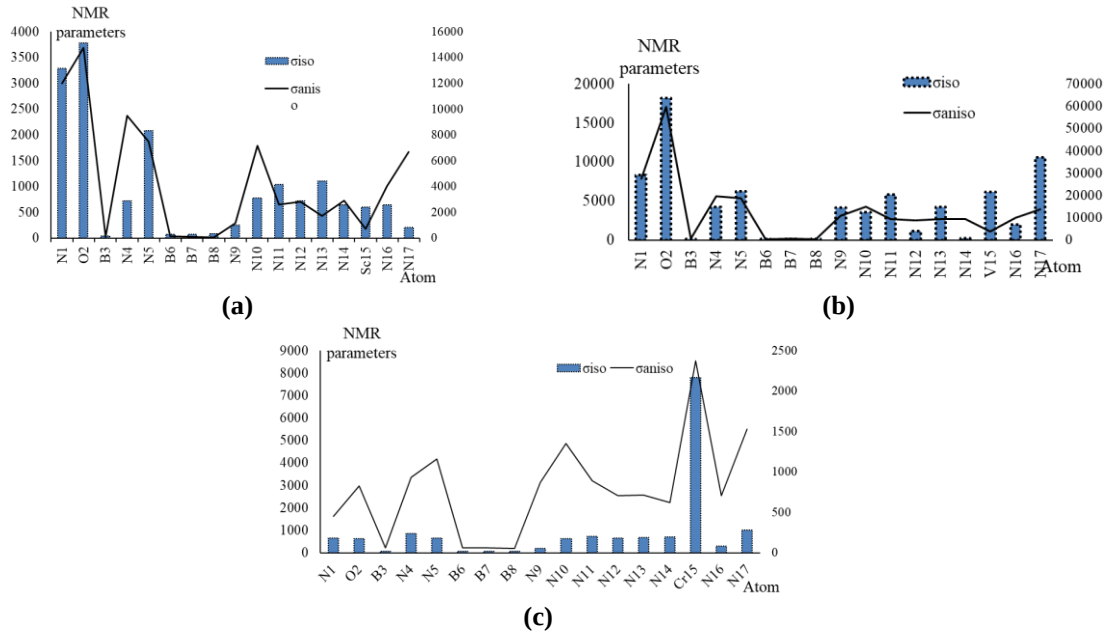

Figure 4. The NMR spectra for **(a)** NO@B_4**(**Sc**)**N_{10}; **(b)** NO@B_4**(**V**)**N_{10}; **(c)** NO@B_4**(**Cr**)**N_{10} complexes using CAM–B3LYP–D3/6-311+G (d,p), LANL2DZ. (Note: the sign of adsorption is shown with @).

In Figure 4 (a,b,c), gas molecules of NO in the complexes of NO@B_4**(**Sc**)**N_{10} (Figure 4a), NO@ B_4**(**V**)**N_{10} (Figure 4b), and NO@B_4**(**Cr**)**N_{10} (Figure 4c) denote the fluctuation in the chemical shielding during gas trapping.

Figure 4 (a,b,c) shows the gap chemical shielding between scandium, vanadium, and chromium doping of B_4**(**X**)**N_{10} nanocage and NO gas molecules. The yield of electron accepting for doping atoms on the B_4**(**X**)**N_{10} through gas molecules adsorption can be ordered as: Cr>V≈SC, which approves the possibility of a covalent bond between scandium, vanadium, chromium, and nitrogen monoxide towards removing it from the air.

In NMR spectroscopy, the remarkable peaks around the interaction of NO molecules through adsorption on the B_4**(**X**)**N_{10} have been observed during toxic gas detection and its scavenging from the air; however, there are some fluctuations in the chemical shielding behaviors of isotropic and anisotropic attributes. The nanostructure was developed through initial model construction based on statistical analysis of spectral data. The final two-dimensional nanostructure was confirmed through iterative validation against the ^{14}N NMR spectra. NO molecules and the B_4**(**X**)**N_{10} nanocage units were added or removed with linkage adjustments guided by comparison to the ^{14}N NMR spectrum. The results of the ^{14}N NMR spectral fitting display the proportions of N-containing functional groups in the nitrogen backbone (Figure 4a,b,c).

Therefore, the authors believe that the extracted results would be useful in the design of B_4**(**X**)**N_{10} complexes based on doped nanomaterials for increasing the adsorption of NO gas molecules, in addition to the structural studies using solid-state and solution NMR techniques.

3.4. IR spectroscopy and thermodynamic factors.

The IR calculations [21] have been accomplished for the adsorption of NO molecules by B_4**(**X**)**N_{10} during toxic gas sensing in air. Therefore, it has been simulated the several clusters

containing NO@B_4**(**Sc**)**N_{10} (Figure5a), NO@B_4**(**V**)**N_{10} (Figure5b), and NO@B_4**(**Cr**)**N_{10} (Figure5c) complexes using CAM–B3LYP–D3/6-311+G (d,p), LANL2DZ.

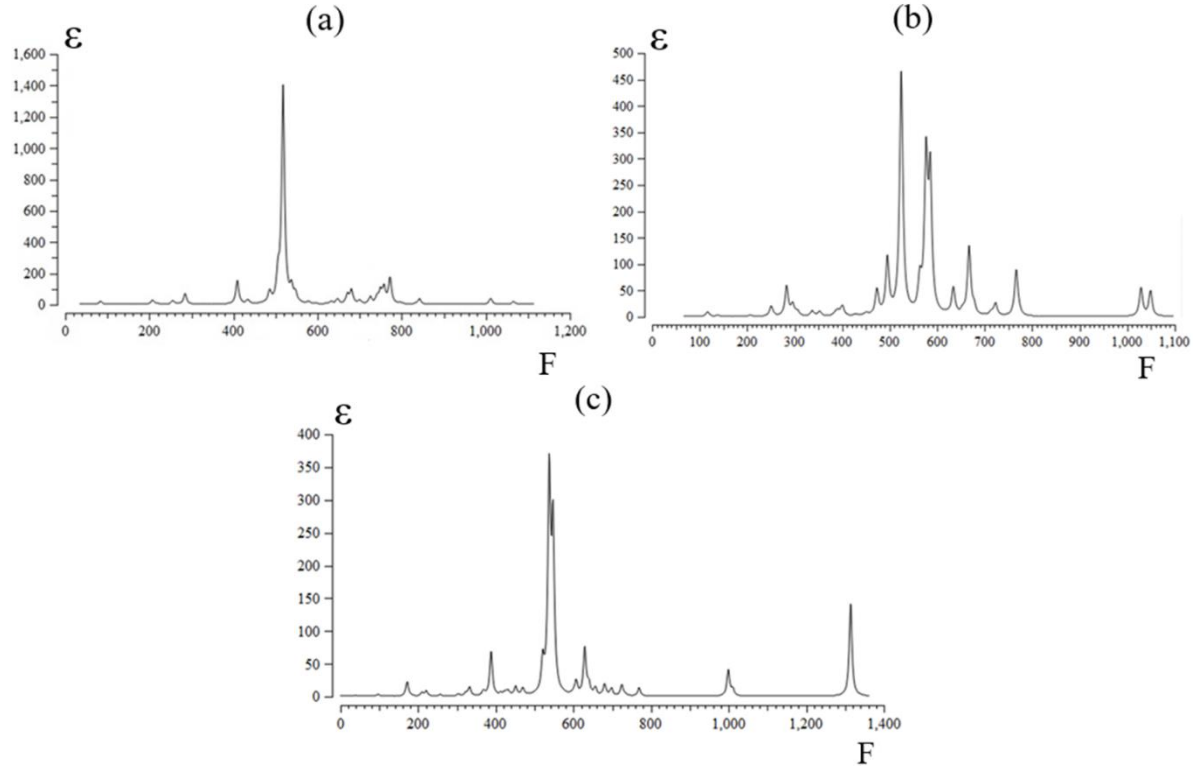

Figure 5. The Frequency (F/cm^{-1}) changes through the IR spectra for **(a)** NO@B_4**(**Sc**)**N_{10}; **(b)** NO@B_4**(**V**)**N_{10}; **(c)** NO@B_4**(**Cr**)**N_{10} complexes using CAM–B3LYP–D3/6-311+G (d,p), LANL2DZ. ε ($M^{-1}cm^{-1}$ or $Lmol^{-1}cm^{-1}$) is the absorbance unit. (Note: the sign of adsorption is shown with @).

The graph of Figure 5 (a) has been observed in the frequency range between 200–1200 cm^{-1} for NO@B_4**(**Sc**)**N_{10} with a sharp peak around 517.89 cm^{-1}. Figure 5 (b) shows the frequency range between 200–1100 cm^{-1} for NO@B_4**(**V**)**N_{10} with sharp peaks around 576.51, 585.20, and 666.98 cm^{-1}. Figure 5 (c) indicates the fluctuation of frequency between 100–1400 cm^{-1} for NO@B_4**(**Cr**)**N_{10} with several sharp peaks around 537.56, 547.52, and 1314.38 cm^{-1}. The IR spectra of NO adsorption on the B_4**(**X**)**N_{10} have demonstrated that the structure of the dominant complex correlates with the electron potency of doped X (X= Sc, V, Cr) on the B_5N_{10}. As it has been seen, the doped nanocages of B_4**(**Sc**)**N_{10}, B_4**(**V**)**N_{10}, and B_4**(**Cr**)**N_{10} complexes have the most fluctuations and the highest tendency for adsorption of NO around 450 cm^{-1}. Therefore, it can be found that IR spectroscopy of NO-adsorbed B_4**(**X**)**N_{10} is now well-placed to address specific questions on the individual effect of charge carriers (gas molecule-nanocage), as well as doping atoms on the overall structure (Figure 5a, b, c).

Table 3, through the thermodynamic specifications, concluded that B_4**(**X**)**N_{10}, due to the adsorption of NO, might be more efficient sensors for detecting and removing the gas molecules from the polluted air.

Table 3. The thermodynamic characters of NO@B_4**(**Sc**)**N_{10}, NO@B_4**(**V**)**N_{10} and NO@B_4**(**Cr**)**N_{10} complexes using CAM–B3LYP–D3/6–311+G (d,p), LANL2DZ calculation.

Compound	$\Delta E^o \times 10^{-3}$ (kcal/mol)	$\Delta H^o \times 10^{-3}$ (kcal/mol)	$\Delta G^o \times 10^{-3}$ (kcal/mol)	S^o (cal/K.mol)	Dipole moment (Debye)
NO@ B_4**(**Sc**)**N_{10}	–515.66	–515.66	–515.69	100.31	0.930
NO@ B_4**(**V**)**N_{10}	–531.30	–531.30	–531.33	105.21	0.350
NO@ B_4**(**Cr**)**N_{10}	–540.96	–540.96	–540.99	111.98	0.780

The thermodynamic parameters of NO gas molecules adsorption on the B_4**(**X**)**N_{10} have been determined using the DFT theoretical technique. It has been shown that for a given number of nitrogen donor sites in NO, the stabilities of complexes owing to doping atoms of Sc, V, Cr, Co, Cu, Zn can be considered as: NO@B_4**(**Cr**)**N_{10}>NO@B_4**(**V**)**N_{10}>NO@ B_4**(**Sc**)**N_{10} (Table 3).

The thermodynamic data in Figure 6 could detect the maximum efficiency of Sc, V, and Cr atoms doping of B_5N_{10} for gas molecules adsorption through ΔG_R^o which depends on the covalent bond between NO gas molecules and B_4**(**X**)**N_{10} as a potent sensor for air pollution removal.

The adsorption process of NO gas molecules on the B_4**(**X**)**N_{10} is affirmed by the ΔG_{ads}^o quantities:

$$\Delta G_{ads}^o = \Delta G_{NO@B4(X)N10}^o - \left(\Delta G_{NO}^o + \Delta G_{B4(X)N10}^o\right); \text{Sc, V, Cr} \quad (3)$$

Table 3 shows that the key role of doped atoms of Sc, V, and Cr during interaction between the adsorbates of NO gas molecules as the electron donors and the adsorbent of B_4(Sc)N_{10}, B_4(V)N_{10}, and B_4(Cr)N_{10} as electron acceptors. Therefore, the selectivity of atom-doping on boron nitride nanocage (gas sensor) for gas molecules adsorption can be summarized as: Cr>V> Sc (Table 3). To elucidate the molecular-level factors governing interfacial stability, we systematically examined the adsorption of NO molecules on a B_4(Sc)N_{10}, B_4(V)N_{10}, and B_4(Cr)N_{10} surfaces. These insights highlight the critical role of both molecular identity and orientation in determining the interfacial behavior of solid surfaces, providing guidance for the rational selection and design of transition-metal-doped B4N10 nanostructures.

4. Conclusions

NO gas molecule separation involving the B_4**(**X**)**N_{10} has been experimented with based on electrostatic interactions between the gas molecules and B_4**(**X**)**N_{10}. The electromagnetic and thermodynamic properties of B_4**(**X**)**N_{10} complexes were computed using density functional theory. The results have illustrated that chosen gas molecules adsorbed on the B_4**(**X**)**N_{10} are rather stable, with the most stable adsorption site being in the center of the B_4**(**X**)**N_{10} system. The selectivity of atom-doping on boron nitride nanocage (gas sensor) for gas molecules adsorption can be expressed as: NO@B_4**(**Cr**)**N_{10} > NO@B_4**(**V**)**N_{10} > NO@B_4**(**Sc**)**N_{10}, respectively. This work proposes that transition metals as ferromagnetic semiconductors can be examined through doping on the nanomaterials for enhancing the adsorption potency towards designing pollution removal sensors. All in all, this research article illustrates how a simple slab-based simulation platform, when combined with well-chosen electronic and energetic descriptors, can capture and recognize the interfacial reactivity trends associated with these gas molecules. This prepares a computationally efficient screening platform to evaluate probable surface stability.

Institutional Review Board Statement

Not applicable.

Informed Consent Statement

Not applicable.

Data Availability Statement

Data supporting the findings of this study are available upon reasonable request from the corresponding author.

Funding

This research received no funding.

Acknowledgments

The author is grateful to Kastamonu University for successfully completing this paper and its research.

Conflict of Interest

The author declares no conflict of interest.

References

1. Alamro, A.; Balbaied, T. Boron Nitride Nanostructures (BNNs) Within Metal–Organic Frameworks (MOFs): Electrochemical Platform for Hydrogen Sensing and Storage. *Analytica* **2024**, *5*, 599–618, https://doi.org/10.3390/analytica5040040.
2. Shtansky, D.V.; Matveev, A.T.; Permyakova, E.S.; Leybo, D.V.; Konopatsky, A.S.; Sorokin, P.B. Recent Progress in Fabrication and Application of BN Nanostructures and BN-Based Nanohybrids. *Nanomaterials* **2022**, *12*, 2810, https://doi.org/10.3390/nano12162810.
3. Yang, Y.; Peng, Y.; Saleem, M.F.; Chen, Z.; Sun, W. Hexagonal Boron Nitride on III–V Compounds: A Review of the Synthesis and Applications. *Materials* **2022**, *15*, 4396, https://doi.org/10.3390/ma15134396.
4. Mateti, S.; Sultana, I.; Chen, Y.; Kota, M.; Rahman, M.M. Boron Nitride-Based Nanomaterials: Synthesis and Application in Rechargeable Batteries. *Batteries* **2023**, *9*, 344, https://doi.org/10.3390/batteries9070344.
5. Revabhai, P.M.; Singhal, R.K.; Basu, H.; Kailasa, S.K. Progress on boron nitride nanostructure materials: properties, synthesis and applications in hydrogen storage and analytical chemistry. *J. Nanostruct. Chem.* **2023**, *13*, 1-41, https://doi.org/10.1007/s40097-022-00490-5.
6. Wasilewska, M.; Derylo-Marczewska, A.; Marczewski, A.W. Equilibrium and Kinetic Studies on Adsorption of Neutral and Ionic Species of Organic Adsorbates from Aqueous Solutions on Activated Carbon. *Molecules* **2024**, *29*, 3032, https://doi.org/10.3390/molecules29133032.
7. Magalhães, I.O.; Rodrigues, N.M.; Machado, D.F.S.; Laranjeira, J.A.; Sambrano, J.R.; Martins, J.B. Adsorption of H_2S and SO_2 in IRMOF-1: a computational study using DFT and GCMC simulations. *J. Mol. Model.* **2025**, *31*, 312, https://doi.org/10.1007/s00894-025-06533-2.
8. Hernández-Oramas, M.; Navarro-Ibarra, D.C.; Franco-Luján, V.A.; Román-Doval, R.; Toledo-Toledo, F.; Ojeda-López, R.; Montejo-Alvaro, F. Transition-Metal $Ni_{6-x}Cu_x$ (x = 0–6)/Hexagonal Boron Nitride Composite for CO Detection: A DFT Study. *J. Compos. Sci.* **2025**, *9*, 510, https://doi.org/10.3390/jcs9090510.
9. Kim, D.-H.; Kim, D.; Kim, G.T.; Kim, H.-D. First-principles study of NO adsorption on defective hexagonal boron nitride monolayer. *Surface Sci.* **2024**, *742*, 122448, https://doi.org/10.1016/j.susc.2023.122448.
10. Zhang, X.; Chen, C.; Cheng, T.; Yang, Y.; Liu, J.; Zhu, J.; Hou, B.; Xin, X.; Wen, M. Optimizing the Local Charge of Graphene via Iron Doping to Promote the Adsorption of Formaldehyde Molecules—A Density Functional Theory Study. *Coatings* **2023**, *13*, 2034, https://doi.org/10.3390/coatings13122034.
11. Feng, H.; Cheng, Z.; Lu, Z.; He, Q. Advances in DFT-Based Computational Tribology: A Review. *Lubricants* **2025**, *13*, 483, https://doi.org/10.3390/lubricants13110483.
12. Frisch, M.J.; Trucks, G.W.; Schlegel, H.B.; Scuseria, G.E.; Robb, M.A.; Cheeseman, J.R.; Scalmani, G.; Barone, V.; Petersson, G.A.; Nakatsuji, H.; Li, X.; Caricato, M.; Marenich, A.V.; Bloino, J.; Janesko, B.G.; Gomperts, R.; Mennucci, B.; Hratchian, H.P.; Ortiz, J. V.; Izmaylov, A. F.; Sonnenberg, J.L.; Williams-Young, D.; Ding, F.; Lipparini, F.; Egidi, F.; Goings, J.; Peng, B.; Petrone, A.; Henderson, T.; Ranasinghe, D.; Zakrzewski, V.G.; Gao, J.; Rega, N.; Zheng, G.; Liang, W.; Hada, M.; Ehara, M.; Toyota, K.; Fukuda, R.; Hasegawa, J.; Ishida, M.; Nakajima, T.; Honda, Y.; Kitao, O.; Nakai, H.; Vreven, T.; Throssell, K.;

Montgomery, J.A., Jr.; Peralta, J.E.; Ogliaro, F.; Bearpark, M.J.; Heyd, J.J.; Brothers, E.N.; Kudin, K.N.; Staroverov, V.N.; Keith, T.A.; Kobayashi, R.; Normand, J.; Raghavachari, K.; Rendell, A.P.; Burant, J.C.; Iyengar, S.S.; Tomasi, J.; Cossi, M.; Millam, J.M.; Klene, M.; Adamo, C.; Cammi, R.; Ochterski, J.W.; Martin, R.L.; Morokuma, K.; Farkas, O.; Foresman, J.B.; Fox, D.J. Gaussian 16, Revision C.01, Gaussian, Inc., Wallingford CT, **2016**.

13. Dennington, R.; Keith Todd, A.; Millam John, M. GaussView, Version 6.06.16. Semichem Inc., Shawnee Mission, KS, USA, **2016**.
14. Adekoya, D.; Qian, S.; Gu, X.; Wen, W.; Li, D.; Ma, J.; Zhang, S. DFT-guided design and fabrication of carbon-nitride-based materials for energy storage devices: a review. *Nano-Micro Lett.* **2021**, *13*, 13, https://doi.org/10.1007/s40820-020-00522-1.
15. Kohn, W.; Sham, L.J. Self-Consistent Equations Including Exchange and Correlation Effects. *Phys. Rev.* **1965**, *140*, A1133–A1138, https://doi.org/10.1103/PhysRev.140.A1133.
16. Zhou, J.; Doi, M. Derivation of Two-Fluid Model Based on Onsager Principle. *Entropy* **2022**, *24*, 716, https://doi.org/10.3390/e24050716.
17. Doi, M. The Onsager principle in polymer dynamics. *Prog. Polym. Sci.* **2021**, *112*, 101339, https://doi.org/10.1016/j.progpolymsci.2020.101339.
18. Trontelj, Z.; Pirnat, J.; Jazbinšek, V.; Lužnik, J.; Srčič, S.; Lavrič, Z.; Beguš, S.; Apih, T.; Žagar, V.; Seliger, J. Nuclear Quadrupole Resonance (NQR)—A Useful Spectroscopic Tool in Pharmacy for the Study of Polymorphism. *Crystals* **2020**, *10*, 450, https://doi.org/10.3390/cryst10060450.
19. Hansen, P.E. The synergy between Nuclear Magnetic Resonance and density functional theory calculations. *Molecules* **2024**, *29*, 336, https://doi.org/10.3390/molecules29020336.
20. Gerothanassis, I.P.; Kupka, T. New Insights into Nuclear Magnetic Resonance (NMR) Spectroscopy. *Molecules* **2025**, *30*, 1500, https://doi.org/10.3390/molecules30071500.
21. Butt, M.A.; Juchniewicz, M.; Słowikowski, M.; Kozłowski, Ł.; Piramidowicz, R. Mid-Infrared Photonic Sensors: Exploring Fundamentals, Advanced Materials, and Cutting-Edge Applications. *Sensors* **2025**, *25*, 1102, https://doi.org/10.3390/s25041102.

Publisher's Note & Disclaimer